Stochastic Simulation of the Transducin GTPase Cycle

S. Felber,*# H. P. Breuer,# F. Petruccione,# J. Honerkamp,# and K. P. Hofmann*
*Institut für Medizinische Physik und Biophysik, Medizinische Fakultät Charité der Humboldt-Universität zu Berlin, D-10098 Berlin, and #Fakultät für Physik, Albert-Ludwigs-Universität, D-79104 Freiburg im Breisgau, Germany

ABSTRACT On rod disc membranes, single photoactivated rhodopsin (R*) molecules catalytically activate many copies of the G-protein (G_t), which in turn binds and activates the effector (phosphodiesterase). We have performed master equation simulations of the underlying diffusional protein interactions on a rectangular 1-μm^2 model membrane, divided into 15×15 cells. Mono- and bimolecular reactions occur within cells, and diffusional transitions occur between (neighboring) cells. Reaction and diffusion constants yield the related probabilities for the stochastic transitions. The calculated kinetics of active effector form a response that is essentially determined by the stochastic lifetime distribution of R* (with characteristic time τ_{R^*}) and the reaction constants of G_t activation. Only a short τ_{R^*} (~0.3 s) and a high catalytic rate (3000–4000 $G_t\ s^{-1}R^{*-1}$) are consistent with electrophysiological data. Although R* shut-off limits the rise of the response, the lifetime distribution of free R* is not translated into a corresponding variability of the response peaks, because 1) the lifetime distribution of catalytically engaged R* is distorted, 2) small responses are enlarged by an overshoot of active effector, and 3) larger responses tend to undergo saturation. Comparison of these results to published photocurrent waveforms may open ways to understand the relative uniformity of the rod response.

INTRODUCTION

Living cells respond to external signals through specialized membrane-bound transducer systems. In G-protein-coupled systems, the activation of a receptor protein by an external physical or chemical stimulus initiates a cascade of protein-protein interactions. First, the receptor activates the G-protein by catalyzing guanine nucleotide exchange in a transient receptor-G-protein complex. Then, the G-protein in its active, GTP-binding form binds to an effector protein (e.g., an enzyme or channel). The signal leaves the membrane, at which time the effector mobilizes a second messenger such as cyclic nucleotide or Ca^{2+} ion.

The visual cascade, found on the disc membranes within the retinal rod outer segment, is a well studied example of a G-protein cascade of reactions. It consists of the photoreceptor rhodopsin (R), the G-protein transducin (G_t), and a phosphodiesterase (PDE) effector, which hydrolyzes cytosolic cyclic GMP. Characteristic for the visual system is the detection of single photons with high fidelity. A crucial element thereby is particle amplification, i.e., a single photoactivated receptor can rapidly transmit the light signal to many copies of the G-protein (Fung et al., 1981; Liebman and Pugh, 1979). The experimental results have supported the random walk amplifier concept (Liebman and Pugh, 1979) in which the proteins are understood as freely diffusing particles on the two-dimensional disc surface, allowing photoactivated rhodopsin (R*) to sequentially encounter and activate many molecules of G_t. Each of the active G_t molecules, generated along the R* diffusion path, has then a chance to bind to an effector molecule and to activate it.

As long as the effector enzyme is kept active by a sufficient amount of active G-protein, the light signal is transmitted to cGMP-dependent channels in the plasma membrane. Deactivation of this transducer system implies the shut-off of receptor, G-protein, and effector. G_t and PDE are deactivated in concert by the intrinsic GTPase activity of the G-protein; it is important to note that this deactivation leads to recycling and de novo activation of G-protein, as long as the receptor remains in its catalytically active form. By contrast, deactivation of rhodopsin is a real shut-off, in that the inactive from of rhodopsin can only return into the reactivatable form by a slow regeneration process. Rhodopsin deactivation is brought about by phosphorylation via a rhodopsin kinase and subsequent binding of a molecule of arrestin. The lifetime for any individual active molecule of rhodopsin ends with the binding of arrestin, as the phosphorylation step as such does not reduce much the catalytic capacity (for a review, see Heck and Hofmann, 1993).

The approach applied in this study is mesoscopic (van Kampen, 1981) and thus different from previous macroscopic (Lamb and Pugh, 1992; Kahlert and Hofmann, 1991) and microscopic (see below) approaches. Understanding the visual cascade on a microscopic level would require the knowledge and adequate description of all of the protein-protein interactions involved and the complete reconstruction of the cellular response from these individual interactions. A description in such detail would imply the solution of the equation of motion for all particles, an impossible task in practice. On a macroscopic level, the diffusion equation and chemical rate equations yield an adequate description (Lamb and Pugh, 1992). Differential equations are, even for complex systems, accessible to numerical

Received for publication 10 July 1996 and in final form 27 September 1996.

Address reprint requests to Dr. K. P. Hofmann, Medizinische Fakultät Charité der Humbolt-Universität zu Berlin, Institut für Medizinische Physik und Biophysik, Ziegelstrasse 5–9, D-10098 Berlin, Germany. Tel.:030-2802-6141; Fax: 030-2802-6377; E-mail: hofmann@rz.charite.hu-berlin.de.

0006-3495/96/12/3051/13 $2.00

evaluation (for a simple treatment, see Kahlert and Hofmann, 1991; Pulvermüller et al., 1993). However, the important condition for a macroscopic description is that the particle numbers are large enough and can be treated as continuous variables. This condition is not met, when only a few rhodopsin molecules are activated per second in the working condition of the rod cell.

The mesoscopic approach (van Kampen, 1981; Gillespie, 1992) takes into account the discrete character of the dynamic variables and the resulting fluctuations. The stochastic techniques used here have been worked out as a general tool to analyze complex chemical reaction systems (Breuer et al., 1992a,b). The mesoscopic approach neglects any detail of intra- or intermolecular reaction; protein-protein interaction is approximated by a single step of simultaneous encounter and reaction with a transition rate characteristic for a given pair of proteins. Furthermore, it can be assumed that any reaction or diffusion step is independent of the history of the system, i.e., it satisfies the Markov condition. This will allow us to develop a so-called master equation, which describes the time-dependent probability for any given state of the reaction/diffusion process (for a microscopic foundation, see Gillespie, 1976). We divide the two-dimensional membrane reaction surface into cells (conceivable as rectangles) and describe diffusion by random transitions between neighboring cells. Within each cell, the particles form an ensemble with probabilities for monomolecular and/or bimolecular reactions, characteristic for a given type of particle (e.g., receptor or G-protein). The probabilities can be derived from the macroscopically determined reaction rates (Gillespie, 1976). Previous solutions based on chemical reaction schemes (Kahlert and Hofmann, 1991; Bruckert et al., 1992) will be contained in this description as a limiting case, e.g, for high particle numbers.

Lamb (1994, 1996) has recently considered a more microscopic stochastic model, with the perspective to analyze partial steps of encounter and protein activation during the activation phase of the photoresponse. Our mesoscopic approach is complementary in that it allows us, at the expense of any information about the collisional process, to extend the analysis to the time limit of receptor deactivation. This enables us to incorporate the information that became recently available on the lifetime of active receptor (Pepperberg et al., 1992, 1996; Chen et al., 1995; Langlois et al., 1996) and G-protein (Vuong and Chabre, 1991). The method is also flexible enough to include in the future additional experimental information, for example, that on calcium-dependent regulation (Lagnado and Baylor, 1994).

REACTION MODEL

Some of the protein-protein interactions in the visual cascade have been analyzed in detail and dissected into partial reaction steps (for reviews, see Hofmann and Heck, 1996; Hofmann et al., 1996). As outlined in the Introduction, we will base our analyses on a simple kinetic skeleton of mono- and bimolecular steps, which suffices to establish a reaction scheme (Fig. 1 and Table 1). In the following, we consider the activating and deactivating steps separately.

Activating steps

The multistep conversion of rhodopsin into the active state, taking place within milliseconds after light absorption, is represented by a single (first-order) reaction (step 1 in Table 1 and Fig. 1).

The assumptions on steps 2 (R^*G_t association) and 3 (R^*G_t dissociation) are based on determinations of the speed of G_t activation (Kühn et al., 1981; Vuong et al., 1984; Kahlert and Hofmann, 1991; Pugh and Lamb, 1993) and on kinetic analyses of association and dissociation (Kohl and Hofmann, 1987; Kahlert and Hofmann, 1991; Bruckert et al., 1992). The experimental data indicate an overall rate of production for active, GTP-binding G* of at least 1000 s^{-1}. Light-scattering data and estimations based on the rising phase of the electrical rod response have indicated that the rate can rise to more than 4000 G*/s (Kahlert and Hofmann, 1991; Pugh and Lamb, 1993). We will therefore also consider a case in which both steps 2 and 3 are four times faster, resulting in an overall rate of 4000 G*/s. To account for a possible slowing of step 3 by depletion of GTP, we will also test a much slower dissociation rate. This is not inconceivable because, whenever the

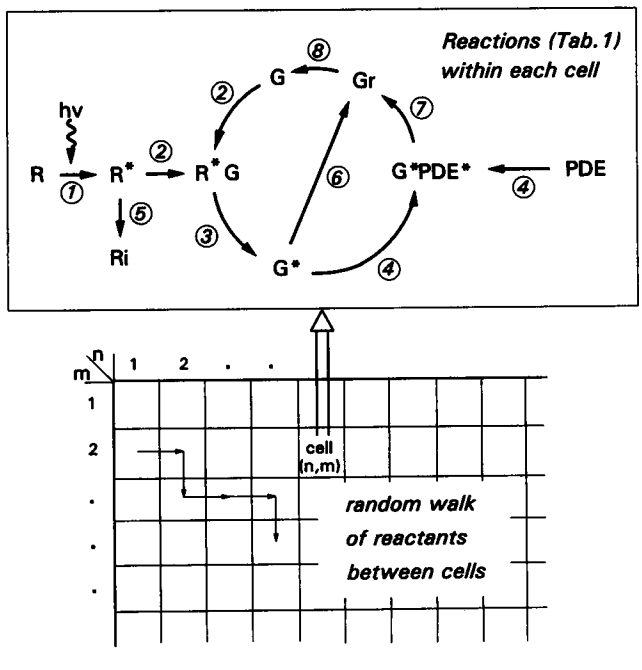

FIGURE 1 Reaction cycle and interactions of G_t. (*Upper panel*) Simplified reaction cycle, showing the reaction steps and species formed. (*Lower panel*) Scheme of the random walk approach to diffusion. All reactions of the scheme above take place within each cell with probability >0, when reactant particles are present. Gain and loss of reactants occur by random transitions of particles between neighboring cells. Probabilities of reaction and cell-cell transition were derived from reaction rates in Table 1 and from diffusion constants (see text).

TABLE 1 Rate constants used in simulations

Reaction	k	Description
Activation		
1. $R \rightarrow R^*$	$200\ s^{-1}$	Transition of R into an active state R*
2. $R^* + G \rightarrow R^*G$	a. $0.75\ \mu m^2(Ns)^{-1}$ b. $3\ \mu m^2(Ns)^{-1}$	Coupling of R* to G_t
3. $R^*G \rightarrow R^* + G^*$	a. $2000\ s^{-1}$ b. $8000\ s^{-1}$	Dissociation of R^*G_t, leaving free R* and active, GTP-bound G*
4. $G^* + PDE \rightarrow G^*PDE^*$	$0.3\ \mu m^2(Ns)^{-1}$	Formation of G*PDE*, the cGMP-hydrolyzing effector enzyme
Deactivation		
5. $R^* \rightarrow R_i$	a. $0.5\ s^{-1}$ b. $3.3\ s^{-1}$	Transition of R* to inactive R_i
6. $G^* \rightarrow G_r$	$0.05\ s^{-1}$	Transition of G_t into a refractory state G_r
7. $G^*PDE^* \rightarrow PDE + G_r$	$2\ s^{-1}$	Dissociation of G*PDE*, leaving inactive PDE and G_r
Reset		
8. $G_r \rightarrow G$	$2\ s^{-1}$	Recycling of G_r

Sources for the rate constants (see text for details) are as follows: step 1, Hofmann et al., 1996; step 2, Kühn et al., 1981; Vuong et al., 1984; Kahlert and Hofmann, 1991; Pugh and Lamb, 1993; step 3, Kohl and Hofmann, 1987; Kahlert and Hofmann, 1991; Bruckert et al., 1992; Pugh and Lamb, 1993; step 4, Heck and Hofmann, 1993; Lamb, 1994, 1996; step 5a, Pepperberg et al., 1992; step 5b, Chen et al., 1995; Langlois et al., 1996; Pulvermüller et al., 1993; Pepperberg et al., 1996; step 6, Antonny et al., 1993; step 7, Vuong and Chabre, 1991; step 8, Hofmann and Heck, 1996. The diffusion constants are from Lamb, 1994, 1996.

concentration of free GTP drops to sub-millimolar concentration, this should affect the G_t activation speed (Kahlert and Hofmann, 1991).

The rate of G*PDE* formation from G* and inactive PDE (step 4) was taken from the measured delay of 5 ms between the formation of G* and its binding to PDE (Heck and Hofmann, 1993). The simplification in this step is considerable, in that the effector in reality comprises two catalytically active subunits, α and β, each bound to an inhibitory γ-subunit. The subunits are successively activated by stoichiometric binding of two GTP-bound G_t α-subunits. The relative activity generated by the partial reactions and the degree of cooperativity between them is still unknown (cf. Hofmann and Heck, 1996). Our assumption of a single rate means an approximation by two independent, equivalent PDE binding sites for G*, which seems to provide a sufficiently good approximation, at least for the activation kinetics (Lamb, 1994, 1996).

Deactivating steps

We will generally assume that a single R* molecule lives for a certain time, t_{R^*}, before it is deactivated in a sudden transition (shut-off). This individual lifetime of a single molecule must be distinguished from the characteristic time τ_{R^*}, which is the inverse of the macroscopic rate of reaction (for the free molecule) and determines the exponential probability distribution of t_{R^*}. The actual value of t_{R^*} was either fixed to a certain value or randomly generated, based on the probability distribution. The procedures are described in the Simulation Techniques.

It is important to note that the effective lifetimes t_{R^*} are prolonged, and the stochastic lifetime distribution is thus distorted (best seen in Figs. 4 and 6), by the fact that the real, response-generating R* spends part of its lifetime in the catalytic complex with G_t. Only in the free intervals does R* have a chance to decay (step 5 in Table 1).

The characteristic times assumed for step 5 are $\tau_{R^*} = 2$ s (5a) and 0.3 s (5b), based on recent electrophysiological studies. $\tau_{R^*} = 2$ s is obtained when the falling phase of the electrophysiological rod response is evaluated under saturating conditions (Pepperberg et al., 1992). However, under conditions of single quantum excitation (i.e., the conditions of these simulations), the time during which R* effectively activates G_t and PDE is considerably shorter. Possible explanations include that single R* molecules can exert their effect on G_t only within a temporally defined domain or that the characteristic lifetime of R* itself is shorter in this case (Pepperberg et al., 1996). Positive evidence in support of a rapid decay of R*, which limits the rise of the response, was given by Chen et al (1995) and by Langlois et al. (1996); see Discussion for details.

As mentioned in the Introduction, the deactivation of R* may comprise a total of three different reaction steps, namely, binding and activation of rhodopsin kinase, phosphorylation of R*, and binding of arrestin. It is known that the kinase can bind only to active rhodopsin, only to the free molecule, and not during the lifetime of its complex with the G_t (Pulvermüller et al., 1993). Our model assumption of first-order decay of R* to R_i (step 5) is consistent with the information as it assumes deactivation of R* only from free R* and not from R^*G_t. Another point is whether the assumption of single first-order decay of R* is realistic in view of the complex nature of biochemical R* deactivation. The binding steps for both rhodopsin kinase and arrestin are fast (~100-200 ms), according to extrapolations from measurements in vitro. In the case of sufficiently long-lived R*, this would leave phosphorylation as the rate-limiting step

and justify the approximation by a single first-order decay reaction, i.e., an exponential distribution of R* lifetime. In the case of short R* lifetime, the three reaction times could be comparable, and our single-step approximation would give an upper limit of stochastic variability. Note, however, that the molecular nature of the reaction that acts as the pacemaker of R* deactivation is not yet known. Rhodopsin kinase (Pulvermüller et al., 1993) and/or the splice variant of arrestin (so-called p^{44}-protein; Palczewski et al., 1994) could downregulate G_t activation, already before phosphorylation and binding of arrestin occurs.

The characteristic times of G* deactivation must fit into the time frame given by heat production experiments. These have shown that the hydrolysis of cGMP in bovine rod outer segments reaches a stable level after less than 1 s (Vuong and Chabre, 1991). This has been interpreted to mean that a stable level of active PDE is reached within this time. We may further conclude that the majority of G* molecules recycle to the GDP-bound state (paths 6 or 7/8, Fig. 1) with a characteristic time $\tau < 1$ s. Thus, a rate of 2 s^{-1} is assumed for the deactivation via PDE-assisted GTPase for the PDE-bound form of G_t, G*PDE* (step 7).

It is important to note that a fast deactivation rate for the majority of the G-protein does not exclude a small fraction of G* that deactivates with a slower rate. It was indeed found experimentally that the GTPase reaction of isolated G_t (a small fraction of the total G* pool, as we will see) is relatively slow, with a rate of 0.05 s^{-1} (Antonny et al., 1993).

The intermediate refractory state (G_r, between steps 7 and 8) was motivated by the fact that in vitro, activated G_t dissociates into its α- and $\beta\gamma$-subunits; the α-subunit alone may interact with the effector, forming G*PDE* (for a discussion, see Hofmann and Heck, 1996). The time it takes to recombine the G_t holoprotein, required for interaction with the receptor, may thus cause a delay after GTP hydrolysis (step 7). In a few cases, simulations without any refractory period (with a direct decay replacing steps 7 and 8) were performed, with no substantial change in the results (see below).

Interplay between activation and deactivation

The systematics of specific activating and deactivating reaction steps, used above, does not lead to the assignment of unique values for the rise and decay of effector activity. Only the interplay between activating and deactivating reactions can explain the pool behavior of an intermediate species at a given time. For example, it will be shown below that the decay of the active effector G*PDE* depends on the activation rate of G_t. In addition to the molecular parameters t and τ (discussed above for R*), one may consider a pool reaction time, which results from the contributions of several reaction steps.

Concentrations, diffusion constants, and boundary conditions

Lamb (1994, 1996) has studied a microscopic discrete square lattice in which the distance between the centers equals a collision radius. In the mesoscopic grid that we are assuming, the 15 × 15 cells within the reaction space of 1 × 1 μm^2 are small two-dimensional reaction cuvettes rather than fixed sites for reacting molecules. For a few cases, we have studied the difference in the simulations between 400 and 225 cells per surface and found it to be negligible. Importantly, it is not useful in the present model to increase the cell number above 400 because the condition of homogeneity of the master equation (van Kampen, 1981) is then no longer met.

Throughout this study, we start the simulation with 1 R* molecule, 3000 G_t molecules (equals G* at maximum), and 600 independent PDE binding sites (equals G*PDE* at maximum). The diffusion constants used are, in $\mu m^2/s$ (see also Lamb and Pugh, 1992; Lamb, 1994): R*, 0.7; G, 1.2; G*, 1.5; G_r, 1,5; R*G, 0.4; PDE, 0.8; G*PDE*, 0.2.

In the simulation algorithm, reflective boundary conditions were applied. None of the particles can move over the rim of the reaction space, but every try is counted with the time-step ϵ. This assumption was made to mimic the limited reaction space (Liebman et al., 1987) made up by the surface and rim of a small disc, as it is found in the retinal rods of warm-blooded animals.

MASTER EQUATION

The reaction steps in Table 1 form a reaction system that provides information about the possible transitions between the species involved. In their original interpretation, the rate constants introduced imply a chemical reaction scheme with a time-dependent space-invariant concentration, i.e., a uniform distribution of a species in space. However, the concentration represents the average value of a discrete quantity, namely, the number of molecules in a surface element dl^2 of the two-dimensional disc membrane surface. The discrete character of the dynamical variables naturally leads to internal fluctuations in the system. Only in a certain limit of large particle numbers may one expect these fluctuations to vanish asymptotically and the reaction-diffusion system still be described by differential equations (Fick's law) and rate constants. As will be shown below, the necessary refinement can be provided by a master equation description on a mesoscopic level.

To formulate this stochastic process, the physical space, i.e., the surface $[0, L]^2$, is discretized into a sufficiently large number M^2 of cells labeled by the integer matrix index (n, m) with n,m = 0, . . . ,M. Doing so, we define a mesoscopic length scale $\delta l = L/M$, which has to be chosen in such a way that the condition of a homogeneous master equation is satisfied (see below). Next we introduce for each cell (n, m) a positive integer $N_{n,m;s}$, which denotes the number of molecules of type s (s = 1, . . . ,S), in cell (n, m). These

numbers are regarded as time-dependent random numbers, i.e., the set $\{(N_{1,1;1}(t), \ldots, N_{M,M;S}(t))\}$ for all values of t represents a multivariate stochastic process. Assuming that this is a Markov process, its dynamics is completely specified by giving a master equation for the probability distribution $P(N_{1,1;1}, \ldots, N_{M,M;S}, t)$. The master equation is written in the form

$$\frac{\partial}{\partial t} P = AP,$$

where A is a linear time evolution operator acting on functions of the stochastic variables $(N_{1,1;1}, \ldots, N_{M,M;S})$. The expectation value F of an arbitrary function $F(N_{1,1;1}, \ldots, N_{M,M;S})$ is

$$\langle F(t) \rangle = \sum_{N_{1,1;1}=0}^{\infty} \cdots \sum_{N_{M,M;S}=0}^{\infty} F(N_{1,1;S}, \ldots, N_{M,M;S}) P(N_{1,1;S}, \ldots, N_{M,M;S}, t).$$

In particular, the expectation value

$$c_s(x_{n,m}, t) \equiv \frac{1}{\delta l^2} \langle N_{n,m;s}(t) \rangle$$

represents the average concentration of molecules of sort s in cell (n, m). It has been shown explicitly (Malek Mansour et al., 1981) that, within the limit of high density and infinite particle numbers, the time evolution equation for the concentration derived from a master equation by the Ω-expansion (van Kampen 1981) converges to the system of differential equations given by the macroscopic description.

Now we demonstrate the construction of the time evolution operators A_r for reactive transitions and A_d for diffusive ones. The latter can be treated as a collective random walk (Honerkamp, 1990). The time evolution operator for the full master equation then reads

$$A = A_r + A_d.$$

The following three elementary transitions are the basic constituents of the master equation.

1) For monomolecular reactions

$$a \xrightarrow{k_m} b \quad \text{or} \quad a \xrightarrow{k_m} b + c$$

in cell (n, m), the differential equation for the kinetics at concentration $c_a(t)$ is

$$\frac{\partial c_a(t)}{\partial t} = -k_m c_a(t),$$

where $\dim(k_m) = s^{-1}$ is the dimension of the monomolecular reaction constant k_m. It does not depend on the dimension in space. All reactive transitions can be described as a simultaneous destruction of the educts and creation of the products.

The number of molecules of type a in cell (n, m) is $N_{n,m;a}$. They decay with a reaction rate

$$W_{Z,Z'} = N_{n,m;a} k_m,$$

where $Z = (N_{n,m;a}, N_{n,m;b}, N_{n,m;c})$ is the state before and $Z' = (N_{n,m;a} - 1, N_{n,m;b} + 1, N_{n,m;c} + 1)$ is the state after the transition.

The master equation for the monomolecular process in the cell (n, m) then reads

$$\frac{\partial P(N_{n,m;a}, N_{n,m;b}, N_{n,m;c}, t)}{\partial t} = -k_m N_{n,m;a} P(N_{n,m;a}, N_{n,m;b}, N_{n,m;c}, t) + k_m (N_{n,m;a} + 1) P(N_{n,m;a} + 1, N_{n,m;b} - 1, N_{n,m;c} - 1, t)$$

It consists of a loss and a gain term, which is clearly seen in this notation. To shorten the formulas, it is convenient to introduce an operator E, which acts on discrete functions in the following way

$$E_{n,m;s} F(\ldots, N_{n,m;s}, \ldots) = F(\ldots, N_{n,m;s} + 1, \ldots)$$

$$E^{-1}_{n,m;s} F(\ldots, N_{n,m;s}, \ldots) = F(\ldots, N_{n,m;s} - 1, \ldots).$$

As $N_{n,m;s} = 0$ is a natural boundary of all processes applied here, no negative particle numbers can occur.

Now the time evolution operator for this monomolecular reaction type reads

$$A_{rm} \equiv k_m (E_{n,m;a} E^{-1}_{n,m;b} E^{-1}_{n,m;c} - 1) N_{n,m;a}.$$

2) For bimolecular reactions

$$a + b \xrightarrow{k_b} c \quad \text{or} \quad a + b \xrightarrow{k_b} c + d$$

in cell (n, m):

The differential equation for this case reads

$$\frac{\partial c_a(t)}{\partial t} = -k_b c_a(t) c_b(t).$$

Here, k_b is a bimolecular rate constant with $\dim(k_b) = [(\mu\text{mol/L})s]^{-1}$ in a three-dimensional case and $\dim(k_b) = [(\text{particles}/\mu m^2)s]^{-1}$ for a two-dimensional problem.

The rate of a transition from the state $Z = (N_{n,m;a}, N_{n,m;b}, N_{n,m;c})$ to $Z' = (N_{n,m;a} - 1, N_{n,m;b} - 1, N_{n,m;c} + 1)$ depends on the product of the particle numbers $N_{n,m;a}$ and $N_{n,m;b}$. For the case of reactions upon a surface of order δl^2, we get

$$W_{Z,Z'} = N_{n,m;a} N_{n,m;b} \frac{k_b}{\delta l^2}.$$

The time evolution operator for that bimolecular reaction then reads

$$A_{rb} \equiv \frac{k_b}{\delta l^2} (E_{n,m;a} E_{n,m;b} E^{-1}_{n,m;c} - 1) N_{n,m;a} N_{n,m;b}.$$

3) For a random walk in two dimensions, as mentioned, the reaction surface is divided into M^2 cells, each labeled with the integer matrix index (n, m). Any possible transition can be written as a product of the two elementary operators $E_{n,m}$ and $E^{-1}_{n,m}$. The jump of a particle to another cell is equivalent to the annihilation in one cell and creation in the other. Each particle has the possibility to jump in four directions, i.e., to the four neighboring cells. The jumps are represented by terms $(E_{n',m'}\,E^{-1}_{n,m} - 1)$ where we assign $(n', m') = (n, m + 1)$ to transitions to the right, $(n', m') = (n, m-1)$ to the left, $(n', m') = (n-1, m)$ to the top, and $(n', m') = (n+1, m)$ to the bottom. A_d describes the collective random walk of particles of sorts s = 1, . . . ,S:

$$A_d \equiv \sum_{s=0}^{S} \frac{D^s}{\delta l^2} \sum_{n=0}^{M} \sum_{m=0}^{M} [E^{-1}_{n+1,m;s}E_{n,m;s} + E^{-1}_{n-1,m;s}E_{n,m;s} + E^{-1}_{n,m-1;s}E_{n,m;s} + E^{-1}_{n,m+1;s}E_{n,m;s} - 4]N_{n,m;s}.$$

Now we develop the master equation for the overall stochastic process, including the reaction system (Table 1) with diffusion of all reactants in two space dimensions:

We identify s = 1, . . . ,9 as follows: 1 = R; 2 = G; 3 = PDE; 4 = R*; 5 = R_i; 6 = R*G; 7 = G*; 8 = G_r; 9 = G*PDE*; then, A_d is the time evolution operator for diffusion of all reactants of our model. To set up A, we look at the reaction system in Table 1 and obtain

$$\begin{aligned} A_r = \sum_{n=0}^{M} \sum_{m=0}^{M} \Big[& k_1(E_{n,m;R}E^{-1}_{n,m;R^*} - 1)N_{n,m;R} \\ & + \frac{k_2}{\delta l^2}(E_{n,m;R^*}E_{n,m;G}E^{-1}_{n,m;R^*G} - 1)N_{n,m;R^*}N_{n,m;G} \\ & + k_3(E_{n,m;R^*G}E^{-1}_{n,m;R^*}E^{-1}_{n,m;G^*} - 1)N_{n,m;R^*G} \\ & + \frac{k_4}{\delta l^2}(E_{n,m;G^*}E_{n,m;PDE}E^{-1}_{n,m;G^*PDE^*} - 1)N_{n,m;G^*}N_{n,m;PDE} \\ & + k_5(E_{n,m;R^*}E^{-1}_{n,m;R_i} - 1)N_{n,m;R^*} \\ & + k_6(E_{n,m;G^*}E^{-1}_{n,m;G_r} - 1)N_{n,m;G^*} \\ & + k_7(E_{n,m;G^*PDE^*}E^{-1}_{n,m;G_r}E^{-1}_{n,m;PDE} - 1)N_{n,m;G^*PDE^*} \\ & + k_8(E_{n,m;G_r}E^{-1}_{n,m;G} - 1)N_{n,m;G_r}. \end{aligned}$$

Two different kinds of boundary conditions for the diffusive random walk are applied. For periodic ones, we set the cell index 1 equal to M + 1 and the cell index 0 equal to M. For reflective boundary conditions, diffusive transitions over the boundary of the reaction surface are forbidden, but every try is counted in time with the chosen time-step ϵ.

SIMULATION TECHNIQUES

One advantage of the master equation formulation of a reaction/diffusion process is that the master equation literally translates into a compact and simple numerical simulation algorithm. Basically, the simulation algorithm generates an ensemble of realizations of the stochastic process from which all quantities of interest can be estimated.

Initially, each particle is randomly placed in a cell (n, m), which is selected among the others with equal probability.

The well known simulation algorithm (Gillespie 1976) for one realization consists of three basic steps:

1) Let us assume that at time t the state of the system is given by $(N_{1,1;1}, \ldots, N_{M,M;S})$. In the first step, the time $t + \epsilon$ of the next transition is determined. The total transition rate, as can be read off the master equation, is

$$W_{tot} = \sum_{n=1}^{M} \sum_{m=1}^{M} W_{n,m},$$

where

$$\begin{aligned} W_{n,m} = & 4\left[\sum_{s=1}^{S} \frac{D_s}{\delta l^2} N_{n,m;s}\right] + k_1 N_{n,m;R} + \frac{k_2}{\delta l^2} N_{n,m;R^*}N_{n,m;G} \\ & + k_3 N_{n,m;R^*G} + \frac{k_4}{\delta l^2} N_{n,m;G^*}N_{n,m;PDE} + k_5 N_{n,m;R^*} + k_6 N_{n,m;G^*} \\ & + k_7 N_{n,m;G^*PDE^*} + k_8 N_{n,m;G_r}. \end{aligned}$$

The probability for any transition to occur within the infinitesimal time-step, i.e., the time the system remains in the state $(N_{1,1;1}, \ldots, N_{M,M;S})$ until the next transition occurs, is exponentially distributed. The random number ϵ is generated from the uniformly distributed random number η on the interval [0, 1] with the formula

$$\epsilon = -\frac{1}{W_{tot}} \ln \eta.$$

2) In the second step, the actual transition that is to occur is chosen from all possible ones, and all variables are updated correspondingly. The set of all possible transitions can be divided into groups with label (n, m). Each group (n, m) contains probabilities for reactive transitions inside the group and for diffusive transitions to its neighboring groups. We identify $W_{n,m}$ as such a group. The probability that a certain transition belongs to group (n, m) is $W_{n,m}/W_{tot}$. We first choose the group with this relative probability by applying the rejection method (Honerkamp, 1990). Then we assign disjunct intervals in [0, 1] to each possible transition of group (n, m). Their length is equal to the probability relative to $W_{n,m}$. The intervals thus add up to unity. By choosing a random number in [0, 1], we can now determine the actual transition. The number and type of the transitions of a group depend on the number and type of particles inside.

Performing this transition as indicated (following the boundary conditions) yields the new state.

3) Repeat steps 1 and 2 until the end of the time interval is reached.

The most important quantity with which we deal is

$$N_{s;r}(t) = \sum_{n=0}^{M} \sum_{m=0}^{M} N_{n,m;s;r}(t),$$

where the index r denotes the number of the realization. $N_{s;r}(t)$ describes, for a given realization, the total amount of a species s as a function of time. For the case s = G*PDE*, $N_{s;r}(t)$ will be understood as the response of the model membrane.

RESULTS

Spatiotemporal pattern of effector activation

The spatial and temporal information provided by the stochastic simulations enables us to study whether the R* generates a local accumulation of active PDE along its trajectory. Fig. 2 shows the results for the "a" conditions (Table 1) and an R* lifetime t_{R*} = 1.5 s. The positions of R* are recorded every 50 ms and connected by straight lines. The distances reflect the diffusion constant of R* (0.7 $\mu m^2\ s^{-1}$). In Fig. 2, *a–d*, the instantaneous occupation of the cells by active PDE (density of G*PDE*) is shown on an optical density scale, with a maximum of 7 G*PDE*s per cell. With a total amount of 600 PDE binding sites, the average number of PDEs per cell is 600/225 (~3). It is seen that, in the very beginning, after 0.2 s (a), the activation zone remains close to the trace of R*. After 0.9 s (b), when the R* had preferentially stayed in cells near the lower left corner, some accumulation of active PDE is seen. After 1.25 s (c), the active PDE no longer shows any correlation to the R* trace, and after 1.8 s (d), well after R* shut-off, the excitation is entirely randomized.

Thus, under our conditions, only in the very early phase of G*PDE* generation did the activity remain localized around the trace of the R*. Later, it spread rapidly enough over the membrane surface to randomize spatially, so that no local depletion (burnout) of PDE occurred. We note that this may apply only to the reaction and diffusion parameters chosen, and that a more extended reaction space (simulating the larger discs of cold-blooded animals) may well behave differently.

When the total amount of active effector (G*PDE*) in all cells is counted in each of the 50-ms time intervals and plotted versus time, a rise and decay of activity results, which is characteristic for a given realization. Fig. 2 shows

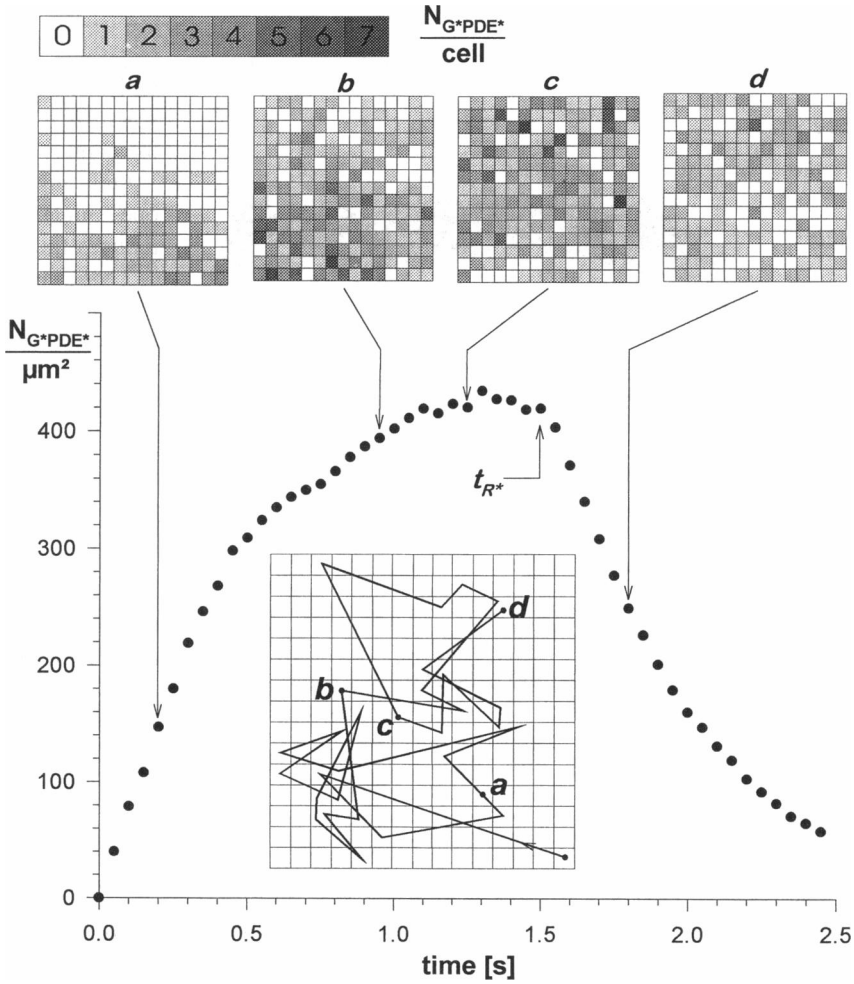

FIGURE 2 Random walk trajectory of R* and spatiotemporal pattern of G*PDE*. (*Inset*) In this example of a realization, R* random walk was started from the lower right corner, position of the R* is shown every 50 ms. The erratic trajectory of R* is replaced by straight lines between these positions. (*Upper panel, a–d*) Density of G*PDE* within each cell, at the times indicated, represented by optical density (scale shown on top). (*Lower panel*) Filled circles show the total number of G*PDE* on the surface as a function of time; arrows indicate the times related to the patterns *a–d* and the lifetime of R*, t_R* in this simulated response of the membrane.

this for the special case considered. It may be predicted that, during the rising phase of such a response, the activating reactions predominate, that the subsequent plateau-like phase reflects a balance between formation and decay of G*PDE*, and that the falling phase reflects dominance of the deactivation reactions. In the following, we will analyze the different phases in more detail.

Families of responses by stochastic variation of R*

Families of responses arise from repeated simulation with one and the same set of parameters. They are similar but show distinct stochastic variability, mainly due to t_{R*}, which varies within the distribution assumed. In Fig. 3, two such families are shown, each with an exponential distribution of t_{R*} around a characteristic time τ_{R*} (0.3 and 2.0 s, respectively).

The responses share a common rising phase. Soon after termination of R* lifetime, they start to decline with an approximately exponential falling phase. For sufficiently long R* lifetime, a plateau level is reached that is, within the limits of the individual fluctuations, the same for all traces. It is obvious that the plateau can be due neither to saturation

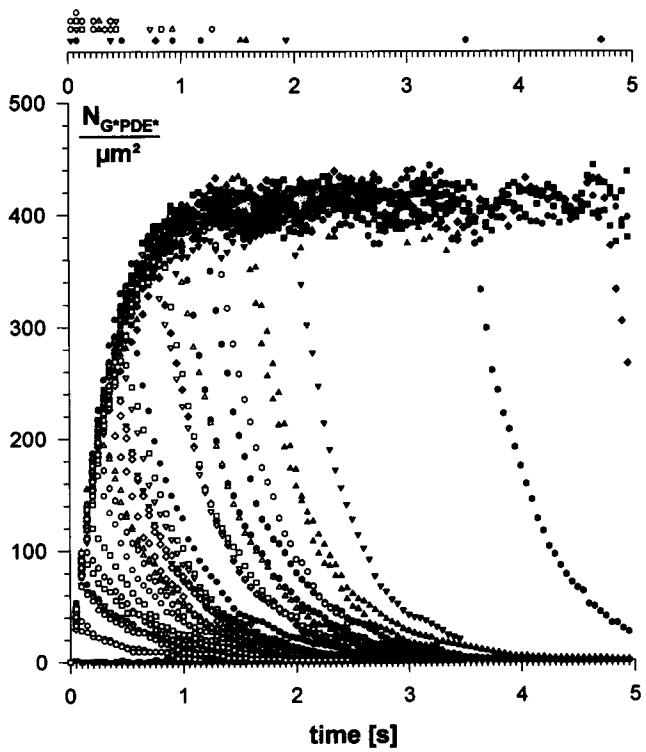

FIGURE 3 Families of responses. In each response, the total amount of G*PDE* on the surface is plotted versus time, for different lifetimes of R*, t_{R*}. Simulations were done with the G-protein activation rates (a) in Table 1. Values of t_{R*} are exponentially distributed with characteristic times τ_{R*}. Filled symbols τ_{R*} = 2 s (step 5a); empty symbols, τ_{R*} = 0.3 s (step 5b). The time scale on top shows t_{R*} for each of the realizations, using the same symbols.

of the available PDE sites (which would be 600) nor to an exhaustion of free, activatable G-protein (see below). It rather reflects the balance between gain and loss of G*PDE*, which is offset when R* is shut off. The onset of the plateau must reflect the point at which the deactivating reactions begin to balance the gradually slowing activation (see below). It could, in principle, be co-determined by local restrictions of the activation process; however, we have seen above that this is not relevant under the assumed conditions.

Rate of G* production determines overall level of active effector

The plateau reflects a limit of effector activity, which cannot be surpassed for single photon excitation and a given set of reaction/diffusion parameters. It is a suitable measure of overall effector activation. Pronounced effects are seen whenever the partial steps of G_t activation are altered; the G* decay reactions are less important in this regard.

A lower plateau arises from faster decay of free G* (a change of the rate from 0.05 to 2 s^{-1} resulted in a 10% lower plateau; data not shown). Enhancing this reaction provides a shunt for free G* back to G_t, so that fewer molecules flow through the PDE branch (steps 4 and 7). With the same reaction rates but faster transitions between the cells (i.e., diffusion) for active and/or inactive G_t, the responses are not significantly altered. This is consistent with the absence of local restriction stated above, as only when such restrictions exist can enhanced diffusion lead to the capture of more particles and enhanced activation.

Omitting the refactory period (replacing steps 7 and 8 by one single G*PDE* decay step with 1-s reaction time) reduces the plateau level of G*PDE* by ~10%.

Lowering the rate of R*G_t dissociation must lower the overall rate of activation. More importantly, it prolongs the lifetime of R* as R* in the R*G complex cannot decay to R_i (see Reaction Model). Fig. 4 shows a family of responses with the parameters of Fig. 3 (τ_{R*} = 0.3), except that the R*G dissociation (step 3 in Fig. 1 and Table 1) was chosen to be five times slower. The plateau is reached after the same time (~1-1.2 s), but it assumes a much lower level. Moreover, the onset of deactivation is now shifted to much longer times. Slowing of R*G dissociation is, in principle, a realistic assumption if the nucleotide metabolism of the cell allows the cofactor GTP to drop below the millimolar concentration required (which, however, does not seem to apply to the functioning rod; see the Discussion).

Effector activation can be driven to the limit where all PDE is saturated when the overall speed of G_t activation is sufficiently enhanced. In Fig. 5, *A* and *B*, two cases (2a, 3a and 2b, and 3b in Table 1) are compared, with a difference by a factor of four in both partial steps of R*-catalyzed G_t activation (steps 2 and 3 in Fig. 1) and a corresponding difference in overall speed of G* generation (1000/s vs. 4000/s). The general observations for G*PDE* are that 1) it rises faster, 2) the plateau is reached more quickly, and 3) it

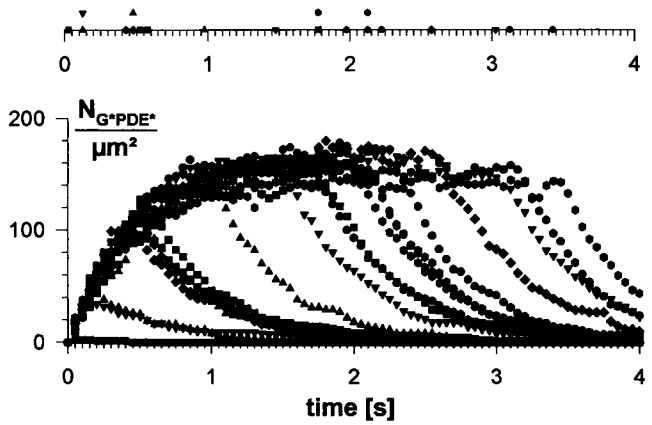

FIGURE 4 Effect of a long-lived R*-G_t complex. The figure shows a family of responses, analogous to Fig. 3 and with the same kinetic parameters (τ_{R^*} = 0.3 s), except that the dissociation of the R*G_t (step 3 in Fig. 1) was chosen to be four times slower (500/s). Note the slow rise and low plateau in these responses; the onset of the falling phase is protracted, despite the short characteristic lifetime of free R*.

virtually assumes the highest possible level (600 G*PDE*s, i.e., the total number of PDE molecules present; Fig. 5 *B*). Comparison of the two cases (1000/s vs. 4000/s) in Fig. 5 *B* shows that, with the more rapid generation of G*, the amount of free G* (active, GTP-bound, but not yet effector-bound G-protein) rises to even higher levels than G*PDE*. In Fig. 5 *C*, the arrows indicate the interval of R* shut-off. It is seen that the amount of G*PDE* continues to rise (for short t_{R^*}, i.e., response amplitudes well below saturation) or stays constant (for long t_{R^*}) after R* was deactivated. This effect (which will be termed overshoot) is a key element in the activation and dynamics of effector activation, as will be shown below.

Specific effects of fast G* production

A closer inspection of Fig. 5 *A* shows that in both cases the rising phase of G*PDE* starts with a sigmoidal shape (Kahlert and Hofmann, 1991) or delayed ramp (Lamb and Pugh, 1992; Lamb, 1996). The solid line is the related numerical solution of the deterministic differential equation system (Kahlert and Hofmann, 1991). The deviation of the stochastic solution from the deterministic approach is rather small in this range, in agreement with the observations of Lamb (1996).

In the slow case, the following observations can be made:

1a) G*PDE* rises almost linearly with time (Fig. 5 *A*, left).

2a) The fraction of free G* remains very small at any time; free G* never accumulates under these conditions (Fig. 5 *B*, left).

3a) G*PDE* starts to drop immediately after shut-off of the R* molecule with a quasi-exponential falling phase, governed by the time constant of G*PDE* decay (step 7); this is best seen in Figs. 2 and 3.

In the fast case, one observes the following:

1b) Free G* rises over several phases; after the initial sigmoidal phase and steep rise, it goes through a phase with reduced rising slope, until G*PDE* has reached saturation (Fig. 5, *B* and *C*, right).

2b) Free G* rises to a level even higher than the G*PDE* plateau (Fig. 5, *B* and *C*, right).

3b) For sufficiently long R* lifetime, G*PDE* does not drop immediately after R* shut-off (Fig. 5 *C*, right) but stays high over 0.5 s, so that the response is considerably prolonged.

4b) For short R* lifetime, the amount of G*PDE* continues to rise after R* shut-off, leading to an overshoot of G*PDE*.

The interpretation of these results is straightforward. In the initial rising phase, when G* molecules are rapidly generated, a substantial amount of free G* can accumulate because the interaction with the PDE becomes rate limiting (step 4). When R* is shut off within this time domain, additional G*PDE* will be formed from these free G* molecules, causing the overshoot of G*PDE* (Fig. 5 *C*, left).

In the plateau phase, when PDE is saturated, G* can again accumulate, because the deactivating reactions (steps 7 and 8) cannot work off G*PDE* rapidly enough. Here one should remember that the excess G* must pass through the G*PDE* state before it can be deactivated, as the direct decay of free G*, step 6, is slow. Only when the free G* approaches zero can G*PDE* be effectively removed and the prolonged response terminated.

Notably, even in the case of fast G* generation, the total amount of active G_t (G* and G*PDE*) never exceeds 50% of the total G_t pool (600 G*PDE* plus 900 G* molecules vs. a total amount of 3000 copies of G-protein; Fig. 5 *B*). The maximal (plateau) amount of G* rises to 1500, when the refractory state is omitted, and a direct decay (replacing steps 7 and 8 by one step with 1 s^{-1}) is assumed (data not shown).

Variability of the responses

Families of responses are shown in Fig. 6. It is clearly seen that the distribution of R* lifetimes is not exponential (see the indicated t_{R^*} on top). This reflects 1) the time it takes to generate R* (5 ms) and 2) the fact that R* engaged in catalytic interaction with G_t cannot decay (competing steps 3 and 5 in Fig. 1 and Table 1). In addition, the overshoot effect for early shut-off, discussed above, causes all of the responses the t_{R^*} of which lie in the first 0.05-s interval to reach ~30% of the maximal (plateau) activation. Both effects together cause a virtual absence of small responses.

Inversely, large responses, i.e., those with sufficiently long R* lifetime, tend to be prolonged by the excess G* formed. This trend continues up to the beginning of a G* plateau (Fig. 5 *C*); it exaggerates the variability imposed by the mere stochastic t_{R^*} distribution.

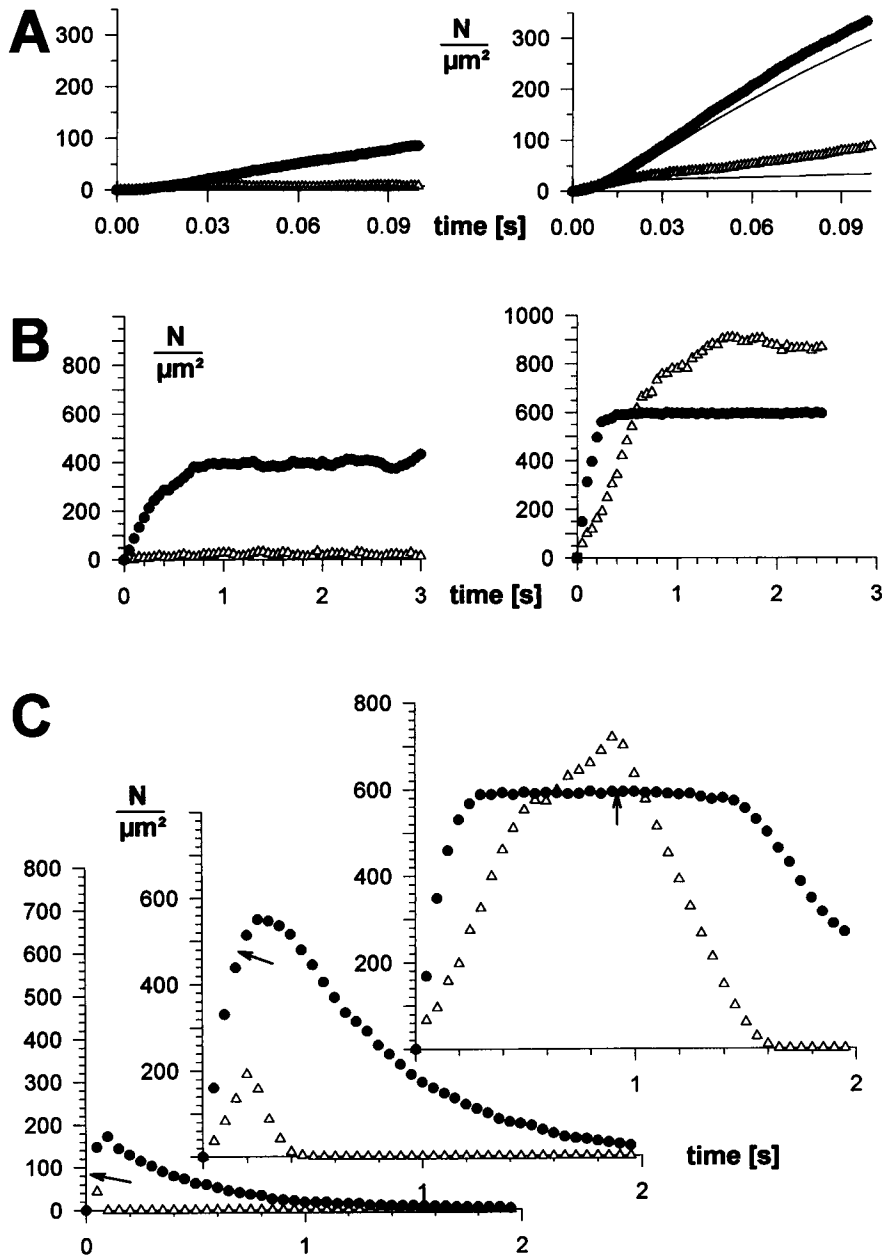

FIGURE 5 Effect of fast G_t-activation. (*A*) Comparison of realizations, using the same rates as in Figs. 2 and 3 (with $\tau_{R^*} = 0.3$ s), or a four times faster G_t activation, i.e., formation and dissociation of R*G complex (*right*), for G*PDE* (●) and for free G* (△). Solid lines are numerical solutions of the deterministic differential equation system (Kahlert and Hofmann, 1991), using the rates of Table 1. (*B*) Same as *A*, on a longer time scale. (*C*) Three realizations of the fast case, for different lifetimes of R*. Arrows indicate the 50-ms time interval, in which R* is shut off (t_R* interval).

Generally, it can be stated that fast G* generation tends to stereotype the peak and to vary the falling phase of the responses.

The resulting variability of the responses is illustrated in Fig. 7. It shows the time course of the average (μ and the normalized μ') of the responses in Fig. 6 and, for comparison, the double of the standard deviation (σ) of an assumed Gaussian distribution. It is seen that the variability at the peak of the response is relatively small (±20%); the maximum of variability (±25%) is reached within the falling phase.

DISCUSSION

This study provides the tools for analyzing full activation/deactivation cycles of the visual cascade. The master equation and simulation techniques applied make use of the fact that the underlying biochemical reaction/diffusion system allows a certain degree of coarse-graining in time and space. This has led to the idea to divide a 1-μm^2 model membrane in reaction cells that are sufficiently small to account for diffusion and large enough for chemical homogeneity. Available data suggest an optimum at 200–400 cells (see Reaction Model). This mesoscopic approach is complementary to the microscopic molecule-by-molecule approximation, as provided by Lamb (1992, 1996). Naturally, the current method must leave the details of collisional coupling and protein-protein interaction out of consideration, as all details of microscopic interaction are summarized into reaction rates. On the other hand, it provides the benefit that the evolution of the system can readily be calculated for a longer time.

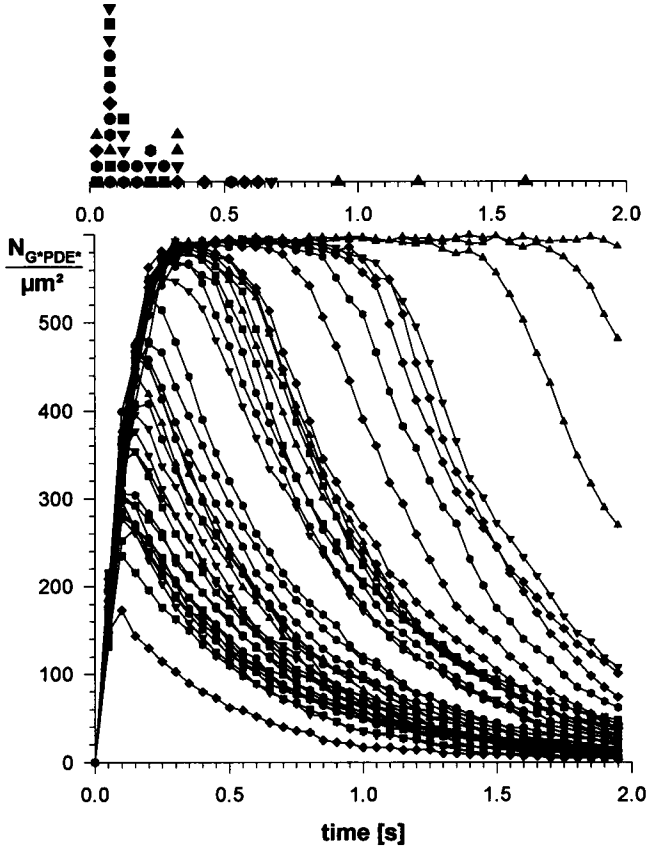

FIGURE 6 Responses with fast G_t activation. Analogous to Fig. 3 (empty symbols), the total amount of G*PDE* on the surface is plotted versus time, for a stochastic ensemble of lifetimes of R*, t_{R*}. But, as in Fig. 5, both the formation and dissociation of the R*G complex are four times faster, leading to fast generation of G*. Values of t_{R*} for free decay of R* are exponentially distributed with characteristic time $\tau_{R*} = 0.3$ s. On the time scale on top, the real t_{R*} (see Reaction Model) are shown for each of the realizations, using the same symbols.

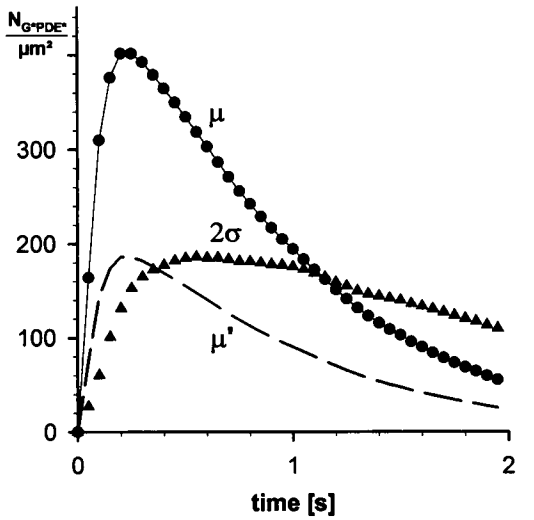

FIGURE 7 Ensemble average and standard deviation of the responses in Fig. 6. The responses in Fig. 6 were point by point averaged; μ denotes the ensemble average and σ the standard deviation of an assumed Gaussian distribution; μ' is the average response, normalized to the maximal amplitude of 2σ.

Based on the experimentally determined reaction rates (Fig. 1; Table 1) and plausible assumptions about the diffusion of the different species, the calculations yield the spatial and temporal distribution of all of the intermediate species involved in the rise and decay of active effector (G*PDE*).

Rise and decay of active effector: the membrane response

The spatial information contained in the realizations (Fig. 2) has allowed us to estimate whether the capacity of an R* molecule to catalyze G-protein activation is spatially restricted. In mammalian rods, the immediate candidate for such a restriction is the surface that represents one side of a disc. This surface is on the order of magnitude of the 1-μm^2 reaction/diffusion space (with reflecting boundary) that we have assumed in our model calculations. Beyond this natural border, spatio-temporal restrictions, for example, by a local depletion of G_t or PDE in the form susceptible to activation (Pepperberg et al., 1996) do not seem to apply, at least within the reach of our analysis and the underlying experimental information. However, we have left out of consideration any time-consuming unproductive encounters, for example, of R* with active G* or G*PDE*. Such effects may play a role and cause some distortion due to local burnout of G-protein and/or effector.

For the rod, we may assume in addition that all active effector molecules, independent of their instantaneous location, equally contribute to the electrical response, because the soluble cytoplasmic messenger cGMP is redistributed rapidly enough on a radial coordinate (Lamb, 1996).

As stated above, the calculated rise and decay of active effector (G*PDE*) may be considered as a synthetic response of the disc membrane.

Only fast G_t activation fits electrophysiological waveforms

Two of the recent electrophysiological studies on retinal rods of warm-blooded animals may be compared with our simulations. Chen et al. (1995) have recorded photocurrents from retinal rods of normal and transgenic mice in which the rhodopsin was mutated in the COOH-terminal region and thus impaired in R* shut-off. Schneeweis and Schnapf (1995) have studied photovoltages from monkey rods. Where the experiments were performed in the single-photon regime, they are comparable to the case simulated in this study. The mutant study (Chen et al., 1995) has shown that, on average, the normal transient responses rise to a peak of ~60% of a maximal plateau amplitude, reached with the long-lived R*. Thus, a sufficiently early R* deactivation limits the rise of the electrical response. The same was

recently found for heat production responses to dim light from isolated rod outer segments (Langlois et al., 1996). We can conclude that the rod response is, well over its peak, determined by R*-dependent factors, i.e., the G-protein cascade. We may compare these normal and prolonged waveforms to our simulations and select a normal average response (see also Fig. 7) in which R* shuts off early enough to make the response transient and one of those in which the plateau is reached (see, for example, Figs. 5 *C* and Fig. 6). Although the photocurrent response and the simulated effector response are separated from each other by a transduction step comprising cGMP binding and hydrolysis (see Lamb, 1996; Hofmann and Heck, 1996), they are similar to one another, both in their time to peak and in the relation between average response and plateau. The falling phase is also comparable, especially the somewhat slower quasi-exponential decays and incidental plateau-like traces found by Schneeweis and Schnapf (1995) .

To obtain the fast rise and short time to peak typical for the electrical waveforms, we have to take the fastest activation of the G-protein that we have assumed (4000 G*/s). A slower activation rate would lead to a too slow rise and late peak of the response.

Rise and decay of active effector depend on the rate of G_t activation

If only fast G_t activation is realistic, this has consequences for the kinetics of the cascade. The comparison above shows that a single photon can drive effector activation on a disc of a mammalian rod well to the limit of saturation (Figs. 5 and 6). Remarkably, a substantial fraction of the G-protein remains thereby inactive; even for the fastest G_t activation assumed, it is still one-third of the total pool (Fig. 5, *B* and *C*). Note that this is not due to a fixed pool of G-protein molecules that remain untouched but arises from the dynamic balance between activating and deactivating reactions. To keep the rate of activation at such a high level, the cellular nucleotide metabolism must afford a high degree of GTP (and GDP) homeostasis.

More importantly, it turns out that the free G-protein that rapidly accumulates in excess of the instantaneously available effector sites is a major element in shaping the response. We have seen that this occurs in two phases of the activation process. The first is in the early rising phase, when the G* rapidly formed cannot bind quickly enough to effector sites. The substantial amount of free G* that accumulates acts as a kinetic buffer when R* is shut off early, and flows into an overshoot of G*PDE* (Fig. 5 *C*, left). The second is in the beginning of the falling phase, when the deactivating reactions (steps 7/8) cannot catch up with the G* formed in excess over the available effector binding sites. The free G* molecules must literally wait for their chance to find a free PDE and to get deactivated. There is a quite sudden transition into this behavior, when the activation speed of G_t rises over a certain limit (~2000 G*/s). The immediate deactivation of free G-protein is slow (characteristic time of 20 s, step 6) and does not contribute much to the falling phase of the response.

Both effects, together with the distortion of the stochastic lifetime distribution of catalytically engaged R* (see above), co-determine the shape of the response. This results in relatively large peaks and, for the few responses from long-lived R*, a prolonged falling phase.

The trend to uniformity of fast G_t activation

The observations outlined in the last paragraph open ways to estimate the variability of the responses. As small and short responses are less likely, the variability at the peak of the responses is smaller than expected from the exponential distribution of the R* lifetime. As we have seen, the interplay of the kinetic constants is such that the response peaks focus in a relatively narrow band near the plateau. This is in remarkable analogy to the behavior of single-photon responses recorded from primate rods, which do not show the degree of variability that would be expected from an exponential lifetime distribution (Baylor et al., 1984). This work opens ways to understand that R* does govern the interruption of the excitatory signal, but a time-dependent overshoot of the signal tends to preserve a constancy of the waveform over the peak of the response.

Interestingly, recent investigations have stated that the falling phase shows enhanced variability with respect to the peak (Schneeweis and Schnapf, 1995). This trend can also be qualitatively verified in our simulations, as prolongation of the falling phase, which increases with R* lifetime, exaggerates the variability imposed by the stochastics of R* itself (Figs. 5–7).

An estimation of R* lifetime in the single photon regime

It is obvious that all of the conclusions above can hold only if the lifetime of R* is on the order of 0.3 s. This is significantly shorter than the 2-s time domain for τ_{R*} obtained from light scattering and electrophysiological rod responses under saturating conditions, i.e., when many R* molecules are simultaneously generated in the reaction space (Pepperberg et al., 1992). However, a more recent investigation, which extended the analysis to lower photoexcitation by using the human electroretinogram, has led to the conclusion (Pepperberg et al., 1996) that the time during which R* can effectively activate G_t and PDE is in this case considerably shorter. The data were interpreted in terms of a rapid decay of active effector, but the possibility of a shorter characteristic lifetime of R* was alternatively considered.

A biochemical basis for a short R* lifetime in the single-photon regime would be provided by rapid competitive binding of excess rhodopsin kinase (Pulvermüller et al., 1993) or of the splice variant of arrestin (p^{44}, Palczewski et

al., 1994), which may block the access of G_t to R* before phosphorylation has occurred. Whether this mechanism plays a role under conditions in vivo remains to be determined.

Future applications of the new technique

The simulations have shown that even a one-step stochastic shut-off, as the one that would arise from a pseudo-first-order competitive binding reaction, leads to a surprisingly high degree of uniformity in the responses. The trend to uniformity can be enhanced when nonexponential, narrower distributions of R* lifetime are generated, for example, by assuming two- or three-step deactivation. Additional improvements of the current model may also include more realistic mechanisms of G-protein/effector interaction and mechanisms of Ca^{2+}-dependent regulation (Lagnado and Baylor, 1994). Such refinement, however, requires a body of biochemical information, which is in these cases not yet complete (Hofmann and Heck, 1996; Hofmann et al., 1996).

In view of the growing knowledge about signal transduction, future analyses may be extended to related biological systems. Questions to be addressed include the origin of transduction noise in sensory cells caused by stochastic fluctuations in the concentration of one of the transducing elements (see, for example, Gold and Lowe, 1995). As one can investigate the fluctuations of the number of particles involved in any of the partial reactions (Breuer et al., 1992a,b), the tools used here should be applicable.

We wish to thank Trevor Lamb and Martin Heck for helpful discussions and Ernst Helmreich and David Pepperberg for comments on the manuscript.

This work was supported by the Deutsche Forschungsgemeinschaft (SFB 60 and SFB 366) and by the Fonds der Chemischen Industrie.

REFERENCES

Antonny, B., A. Otto-Bruc, M. Chabre, and T. M. Vuong. 1993. GTP hydrolysis by purified -subunit of transducin and its complex with the cyclic GMP phosphodiesterase inhibitor. *Biochemistry*. 32:8646–8653.

Baylor, D. A., B. J. Nunn, and J. L. Schnapf. 1984. The photocurrent, noise, and spectral sensitivity of rods of the monkey *Macaca fascicularis*. *J. Physiol.* 357:575–607.

Breuer, H. P., J. Honerkamp, and F. Petruccione. 1992a. Stochastic simulation of polymerization reactions. *Comp. Polymer Sci.* 1:233–240.

Breuer, H. P., J. Honerkamp, and F. Petruccione. 1992b. A stochastic approach to complex chemical reactions. *Chem. Phys. Lett.* 190: 199–201.

Bruckert, F., M. Chabre, and T. M. Vuong. 1992. Kinetic analysis of the activation of transducin by photoexcited rhodopsin: influence of the lateral diffusion of transducin and competition of guanosine diphosphate and guanosine triphosphate for the nucleotide site. *Biophys. J.* 63: 616–629.

Chen, J., C. L Makino, N. S. Peachey, D. A. Baylor, M. I. Simon. 1995. Mechanisms of rhodopsin inactivation in vivo as revealed by a COOH-terminal truncation mutant. *Science*. 267:374–377

Fung, B. K., J. B. Hurley, and L. Stryer. 1981. Flow of information in the light-triggered cyclic nucleotide cascade of vision. *Proc. Natl. Acad. Sci. USA*. 78:152–156.

Gillespie, D. T. 1976. A general method for numerically simulating the stochastic time evolution of coupled chemical reactions. *J. Comp. Phys.* 22:403–434.

Gillespie, D. T. 1992. A rigorous derivation of the chemical master equation. *Physica A*. 188:404–425.

Gold, G. H., and G. Lowe. 1995. Single odorant molecules? *Nature*. 376:27

Heck, M., and K. P. Hofmann. 1993. G-protein-effector coupling: a real-time light-scattering assay for transducin-phosphodiesterase interaction. *Biochemistry*. 32:8220–8227.

Hofmann, K. P., and M. Heck. 1996. Light-induced protein-protein interactions on the rod photoreceptor disc membrane. *Biomembranes*. 2:1–100.

Hofmann, K. P., S. Jäger, and O. P. Ernst. 1996. Structure and function of activated rhodopsin. *Isr. J. Chem.* 35:339–355

Honerkamp, J. 1990. Stochastische Dynamische Systeme. VCH-Verlag, Weinheim, Germany.

Kahlert, M., and K. P. Hofmann. 1991. Reaction rate and collisional efficiency of the rhodopsin-transducin system in intact retinal rods. *Biophys. J.* 59:375–386.

Kohl, B., and K. P. Hofmann. 1987. Temperature dependence of G-protein activation in photoreceptor membranes: transient extra metarhodopsin II on bovine disk membranes. *Biophys. J.* 52:271–277.

Kühn, H., N. Bennett, M. Michel Villaz, and M. Chabre. 1981. Interactions between photoexcited rhodopsin and GTP-binding protein: kinetic and stoichiometric analyses from light-scattering changes. *Proc. Natl. Acad. Sci. USA*. 78:6873–6877.

Lagnado, L., and D. A. Baylor. 1994. Calcium controls light-triggered formation of catalytically active rhodopsin. *Nature*. 367:273–277.

Lamb, T. D. 1994. Stochastic simulation of activation in the G-protein cascade of phototransduction. *Biophys. J.* 67:1439–1454.

Lamb, T. D. 1996. Gain and kinetics of activation in the G-protein cascade of phototransduction. *Proc. Natl. Acad. Sci. USA*. 93:566–570.

Lamb, T. D., and E. N. Pugh, Jr. 1992. A quantitative account of the activation steps involved in phototransduction in amphibian photoreceptors. *J. Physiol.* 449:719–758.

Langlois, G., C. K. Chen, K. Palczewski, J. B. Hurley, and T. M. Vuong. 1996. Responses of the phototransduction cascade to dim light. *Proc. Natl. Acad. Sci. USA*. 93:4677–4682.

Liebman, P. A., K. R. Parker, and E. A. Dratz. 1987. The molecular mechanism of visual excitation and its relation to the structure and composition of the rod outer segment. *Annu. Rev. Physiol.* 49:765–791.

Liebman, P. A., and E. N. Pugh, Jr. 1979. The control of phosphodiesterase in rod disk membranes: kinetics, possible mechanisms, and significance for vision. *Vision Res.* 19:375–380.

Malek Mansour, M., C. van den Broeck, G. Nicolis, J. W. Turner. 1981. Asymptotic properties of Markovian master equations. *Ann. Phys. (NY)*. 131:283–313.

Palczewski, K., J. Buczylko, H. Ohguro, R. S. Annan, S. A. Carr, J. W. Crabb, M. W. Kaplan, R. S. Johnson, and K. A. Walsh. 1994. Characterization of a truncated form of arrestin isolated from bovine rod outer segments. *Protein Sci.* 3:314–324.

Pepperberg, D. R., D. G. Birch, K. P. Hofmann, and D. C. Hood. 1996. Recovery kinetics of human rod phototransduction inferred from the two-branched a-wave saturation function. *J. Optic. Soc. Am. A*. 13: 586–600.

Pepperberg, D. R., M. C. Cornwall, M. Kahlert, K. P. Hofmann, J. Jin, G. J. Jones, and H. Ripps. 1992. Light-dependent delay in the falling phase of the retinal rod photoresponse. *Vision Neurosci.* 8:9–18.

Pugh, E. N., Jr., and T. D. Lamb. 1993. Amplification and kinetics of the activation steps in phototransduction. *Biochim. Biophys. Acta*. 1141: 111–149.

Pulvermüller, A., K. Palczewski, and K. P. Hofmann. 1993. Interaction between photoactivated rhodopsin and its kinase: stability and kinetics of complex formation. *Biochemistry*. 32:14082–14088.

Schneeweis, D. M., and J. L. Schnapf. 1995. Photovoltage of rods and cones in the macaque retina. *Science*. 268:1053–1056.

van Kampen, N. G. 1981. Stochastic Processes in Physics and Chemistry. North Holland, Amsterdam.

Vuong, T. M., and M. Chabre. 1991. Deactivation kinetics of the transduction cascade of vision. *Proc. Natl. Acad. Sci. USA*. 88:9813–9817.

Vuong, T. M., M. Chabre, and L. Stryer. 1984. Millisecond activation of transducin in the cyclic nucleotide cascade of vision. *Nature*. 311: 659–661.